Vol. 3, pp 325–333, Raven Press, New York.
Roussel, A., & Cambillau, C. (1989) in *Silicon Graphics Geometry Partners Directory (Fall 1989)* (Silicon Graphics, Eds.) pp 77–78, Silicon Graphics, Mountain View, CA.
Wagner, G. (1990) *Prog. Nucl. Magn. Reson. Spectrosc. 22*, 101–139.
Wagner, G., & Wüthrich, K. (1982) *J. Mol. Biol. 160*, 343–361.
Wüthrich, K. (1986) *NMR of Proteins and Nucleic Acids*, John Wiley and Sons, New York.
Wüthrich, K. (1989) *Acc. Chem. Res. 22*, 36–44.
Wüthrich, K., Billeter, M., & Braun, W. (1983) *J. Mol. Biol. 169*, 949–961.
Zlotkin, E., Fraenkel, G., Miranda, F., & Lissitzky, S. (1971a) *Toxicon 9*, 1–8.
Zlotkin, E., Rochat, H., Kupeyan, C., Miranda, F., & Lissitzky, S. (1971b) *Biochimie 53*, 1073–1078.
Zlotkin, E., Kadouri, D., Gordon, D., Pelhate, M., Martin, M.-F., & Rochat, H. (1985) *Arch. Biochem. Biophys. 240*, 877–887.

Structural Microheterogeneity of a Tryptophan Residue Required for Efficient Biological Electron Transfer between Putidaredoxin and Cytochrome P-450$_{cam}$†

Patrick S. Stayton and Stephen G. Sligar*
Department of Biochemistry, University of Illinois, Urbana, Illinois 61801
Received July 26, 1990; Revised Manuscript Received November 9, 1990

ABSTRACT: The carboxy-terminal tryptophan of putidaredoxin, the Fe_2S_2·Cys_4 iron–sulfur physiological redox partner of cytochrome P-450$_{cam}$, is essential for maximal biological activity [Davies, M. D., Qin, L., Beck, J. L., Suslick, K. S., Koga, H., Horiuchi, T., & Sligar, S. G. (1990) *J. Am. Chem. Soc. 112*, 7396–7398]. This single tryptophan-containing protein thus represents an excellent system for studying the solution dynamics of a residue directly implicated in an electron-transfer pathway. Steady-state and time-resolved measurements of the tryptophan fluorescence have been conducted across the emission spectrum as a function of redox state to probe potential structural changes which might be candidates for structural gating phenomena. The steady-state emission spectrum (λ_{max} = 358 nm) and anisotropy (α = 0.04) suggest that Trp-106 is very solvent-exposed and rotating partially free of global protein constraints. The time-resolved fluorescence kinetics for both oxidized and reduced putidaredoxin are fit best with three discrete components of approximately 5, 2, and 0.3 ns. The lifetime components were assigned to physical species with iodide ion quenching experiments, where differential quenching of the longer components was observed ($k_{\tau=2}$ = 5.9 × 10^8 M^{-1} s^{-1}, $k_{\tau=5}$ = 1.3 × 10^8 M^{-1} s^{-1}). These findings suggest that the multiexponential fluorescence decay results from ground-state conformational microheterogeneity and thus demonstrate that the essential tryptophan exists in at least two distinguishable conformations. Small differences in the relative proportions of the components between redox states were observed but not cleanly resolved. It thus appears that Trp-106 exists in similar microconformations for both oxidized and reduced putidaredoxin, characterized by three lifetimes with similar relative proportions. These results do not rule out differences within the cytochrome P-450$_{cam}$ complex and indeed suggest potential mechanisms for selection of specific geometries. The absence of fluorescence lifetime wavelength dependencies demonstrates that each species displays the red-shifted, solvent-exposed, steady-state spectra. Differential solvent exposure is thus unlikely to be the primary mechanism for the asymmetric iodide quenching. Differential interactions of the tryptophan microconformations with an anionic protein surface are proposed as a mechanism for the iodide effects and supported by quenching studies with the neutral quenching agent acrylamide. The mechanism is consistent with a physical model of putidaredoxin–cytochrome P-450$_{cam}$ complex formation where the negatively charged surface is suggested to be the anionic binding surface of putidaredoxin implicated in putidaredoxin reductase and cytochrome P-450$_{cam}$ interactions [Stayton, P. S., & Sligar, S. G. (1990) *Biochemistry 29*, 7381–7386]. This model thus places the essential Trp-106 directly at the cytochrome P-450$_{cam}$ binding interface in position to mediate electron transfer.

Biological electron transfer is an extremely complex process that has attracted a great deal of theoretical and experimental effort (Marcus, 1956; Hopfield, 1974; Jortner, 1976; Marcus & Sutin, 1985; Scott et al., 1985; McLendon, 1988). The role of the protein medium in directly modulating biological electron-transfer processes has been the subject of intriguing but relatively fewer experimental and theoretical investigations. Perhaps the most direct demonstration of such a role has been the observation that an aromatic side chain is required at amino acid position 82 in cytochrome *c* for efficient electron transfer to occur with Zn protoporphyrin IX substituted cytochrome *c* peroxidase (Liang et al., 1988). Gray (Therien et al., 1990) and Wolynes (Kuki & Wolynes, 1987) have considered specific through-bond pathways in cytochrome *c* and myoglobin and mutagenesis studies with the blue copper protein azurin have also related electron-transfer kinetics with a specific electron-transfer pathway (van de Kamp et al., 1990). In addition, orientational effects on observed rates,

† This research was supported by National Institutes of Health Grant GM 31756.
* To whom correspondence should be addressed.

0006-2960/91/0430-1845$02.50/0

which imply differential pathways, have been suggested both within the cytochrome *c*–cytochrome *c* peroxidase diprotein electron-transfer complex (Hazzard et al., 1988; Nocek et al., 1990) and within the oxidized and reduced states of covalently modified cytochrome *c* alone (Bechtold et al., 1986).

Conformational gating of electron transfer by dynamic protein motion has been hypothesized to explain some of these rate dependencies (Bechtold et al., 1986; Hoffman & Ratner, 1987; Liang et al., 1988; McLendon et al., 1987; Brunschwig & Sutin, 1989). The gating mechanism in redox reactions may operate with an accompanying conformational change that controls the electron transfer in a two-step process (Hoffman & Ratner, 1987), or by resulting in the production of a different protein matrix between the two redox centers or states, giving directional electron-transfer rates (Bechtold et al., 1986; Brunschwig & Sutin, 1989). These models point to potential governing roles for specific protein residues, although mutagenesis studies have also shown that some residues previously hypothesized to mediate electron transfer either do not, or do not do so uniquely (Miller et al., 1988).

These considerations point to the importance of structural as well as kinetic characterization (Louie et al., 1988). The complexity of the biological electron-transfer rate, which can be affected by a variety of processes including binding kinetics, redox potential shifts, and orientational effects, in addition to the Franck–Condon restricted transfer itself, makes the specific determination of the underlying causes for rate dependencies difficult. The absence of high-resolution crystal data for any diprotein electron-transfer complex makes it impossible at present to directly correlate interprotein kinetics with structure, while the static crystal structures of oxidized and reduced cytochrome *c* at high ionic strength do not reveal an obvious cause for the observed directional intraprotein electron transfer between the heme center and an inorganic complex on the protein surface (Bechtold et al., 1986). At any rate, static crystal structure evidence does not preclude solution dynamics of possible functional importance such as those suggested for Phe-82 in molecular dynamics simulations of cytochrome b_5–cytochrome *c* association (Wendoloski et al., 1987), and in the NMR study of cytochrome b_5–cytochrome *c* diprotein complex formation (Burch et al., 1990).

The observation that an aromatic amino acid side chain is required at the carboxy terminus of putidaredoxin for efficient electron transfer within the physiological putidaredoxin–cytochrome P-450$_{cam}$ complex (Davies et al., 1990a; Sligar et al., 1974) is thus particularly interesting because dynamic structural fluorescence studies in solution of the wild-type C-terminal tryptophan are possible. This system allows for specific structural characterization in terms of tryptophan conformation. Time-resolved measurements of tryptophan fluorescence decay can provide direct information on conformational microheterogeneity (Beechem & Brand, 1985). These measurements can be conducted as a function of redox state to address the question of whether the tryptophan exists in different conformational states when oxidized versus reduced. Such a determination experimentally probes possible mechanisms for the process of conformational gating of electron transfer. While these studies cannot be conducted within the putidaredoxin–cytochrome P-450$_{cam}$ complex (due to the presence of five tryptophan residues in cytochrome P-450$_{cam}$), the effects of redox state on the C-terminal tryptophan have been studied and reveal the first direct evidence of multiple conformational states of a specific side chain necessary for efficient electron transfer within a physiological diprotein complex. In addition, studies utilizing iodide ion as an anionic surface quencher indicate that the putidaredoxin tryptophan is associated with an anionic protein surface. This finding suggests that the tryptophan may lie directly outside the proposed putidaredoxin anionic binding surface (Geren et al., 1986; Stayton et al., 1988; Stayton & Sligar, 1990) in position to mediate electron transfer with cytochrome P-450$_{cam}$.

Materials and Methods

Protein Purification. Putidaredoxin was overproduced in *Escherichia coli* strain TB1 harboring the pUC plasmid derivative pKM 356 which contains the putidaredoxin gene under control of the *lac* promoter (Davies et al., 1990b). The *E. coli* produced protein is identical with that purified from *Pseudomonas putida* by a variety of criteria, including UV–vis spectroscopy, EPR spectroscopy of the one-electron-reduced protein, redox potential measurements, and the ability to turn over cytochrome P-450$_{cam}$ in the reconstituted physiological cytochrome P-450$_{cam}$ electron-transport system. The N-terminal methionine required for *E. coli* expression is processed in vivo to generate the native primary protein sequence (P. Stayton and S. Sligar, unpublished results). Protein was purified according to a slightly modified version of published procedures (Gunsalus & Wagner, 1978). Following cell lysis, the protein was loaded onto a DEAE-cellulose column equilibrated with 50 mM Tris (pH 8.0)–14 mM β-mercaptoethanol (BME) and eluted in the same buffer with a linear 0.0–0.4 M KCl gradient. Pooled fractions were subjected to 35–80% ammonium sulfate salt cuts, and the reconstituted pellet was subsequently loaded onto an ACA-44 gel filtration column (LKB) equilibrated with 50 mM Tris (pH 8.0)–14 mM β-mercaptoethanol. The pooled fractions were then applied to an identical DEAE-cellulose column. Pure protein, demonstrated by homogeneity on an SDS–polyacrylamide gel, yielded an A_{330}/A_{280} ratio of 0.7, comparable to that reported for putidaredoxin purified from *Pseudomonas* (Gunsalus & Wagner, 1978).

Sample Preparation. Putidaredoxin is stable at 20 °C under deoxygenated conditions. Samples of putidaredoxin for fluorescence studies were thus maintained in an anaerobic cuvette allowing evacuation of the protein solution. Putidaredoxin is rapidly (seconds) and quantitatively photoreduced under xenon arc illumination (Schoeffel Universal Arc Lamp Supply, 250 W, water-filtered, 50-cm sample distance) in a buffer consisting of 5 mM EDTA, 3 μM safranin T, and 50 mM Tris, pH 8.0. Control experiments demonstrated that this solution displayed no fluorescence in the 300–400-nm region when excited at 295 nm. The oxidized protein was measured in the same buffer solution with the exception that safranin T was omitted. Quenching experiments utilizing iodide ion and acrylamide were conducted in deoxygenated buffer consisting of 50 mM Tris, pH 8.0. The overall ionic strength at each quencher concentration was kept approximately equal by maintaining a total concentration of potassium and counterion of 266 mM. This was accomplished by addition of KCl in balancing proportions to KI. Photoreduction of putidaredoxin in the presence of iodide proved impossible, and thus the quenching of reduced protein could not be studied. Samples of putidaredoxin for lifetime and steady-state analyses were typically 30 μM in protein. All experiments were conducted at 20 °C.

Fluorescence Studies. Steady state-tryptophan emission spectra were collected on an ISS GREG (Urbana, IL) photon counting instrument and a Hitachi 3010 analogue instrument with excitation at 295 nm. Steady-state polarization measurements were conducted on the ISS instrument. A multifrequency phase and modulation fluorometer utilizing cross-

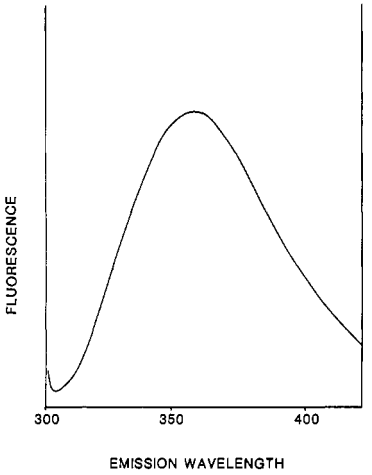

FIGURE 1: Steady-state technical emission spectrum of Trp-106 with excitation at 295 nm.

correlation was used to measure tryptophan lifetimes (Gratton et al., 1984). The laser system consisted of a frequency-doubled (532 nm) mode-locked (38 MHz) neodymium yttrium–aluminum–garnet (Nd-YAG) laser synchronously pumping a cavity-dumped, Rhodamine 6G, single-jet dye laser (Coherent Corp., Palo Alto, CA). The resultant tuned and frequency doubled 295-nm light was polarized at 55°. The frequency range of the exciting light utilized to measure the phase delays and modulation ratios was 2–180 MHz. An ISA monochromator with slits of 1 mm (band-pass 8 nm) was utilized to monitor specified emission wavelengths. *p*-Terphenyl in cyclohexane was used as a reference lifetime (1 ns) to correct for the color shift and instrumental phase delay of the detection equipment.

Analysis of Lifetime Data. Lifetime measurements were analyzed by using a global analysis procedure (Beechem et al., 1990; software package available from Globals Unlimited, Urbana, IL). The fitting algorithm represents a Marquardt–Levenberg nonlinear least-squares analysis using the global matrix mapping approach for parameter linkage (Beechem et al., 1985, 1990). Quenching analysis used a dynamic Stern–Volmer quenching model. Lifetimes were generally analyzed assuming discrete components representing a sums of exponentials model, although distributed fitting was also tested.

RESULTS

Steady-State Analysis. Putidaredoxin contains a single tryptophan residue at its C-terminus, amino acid position 106. The steady-state emission spectrum of Trp-106 is shown in Figure 1. This spectrum indicates that the tryptophan is very solvent-exposed as it is red-shifted to an emission maximum of 358 nm, similar to that of free tryptophan in aqueous solution. The tryptophan anisotropy is 0.040, from which an average rotational correlation time of 5 ns can be calculated by using the Perrin equation and an average lifetime of 2.3 ns. This value suggests that the tryptophan is rotating largely free of global protein constraints since a value of approximately 11 ns would be expected for a protein the size of putidaredoxin as estimated with the Stokes–Einstein equation.

Recovery of Tryptophan Lifetimes and Redox-Linked Dynamics. The time-resolved dynamics of tryptophan-106 were investigated by using multifrequency phase and modulation measurements. The fluorescence decay was fit best with three discrete components. A Lorentzian-distributed fitting analysis gave a best fit with a trimodal model ($\chi^2 = 3.2$), with resolved centers at 4.9 and 2 ns (bandwidths of 0.05 ns) and a short component (centered at less than 0.05 ns) that was very broad (bandwidth 1.5 ns). As this corresponded closely in regard to both fractional intensities and lifetimes to the long- and medium-lifetime components of the discrete model, we utilized discrete fitting to describe the observed fluorescence decay. The oxidized and reduced forms of putidaredoxin independently yielded fits with a long component of approximately 4.7 ns, a median component of approximately 1.7 ns, and a very short component of approximately 0.3 ns. To further define the fitting surface and to obtain the individual spectra associated with each component, the wavelength dependence was characterized. Global analysis linking the three lifetime components across the emission spectra gave χ^2 fits of less than 2 for both the oxidized and reduced forms of putidaredoxin. Because the independent analysis of oxidized and reduced putidaredoxin yielded very similar lifetime components and wavelength dependencies, the two states were combined into one model with the three lifetimes linked across both redox state and the emission spectra. This model gave a global χ^2 of 1.507, with random residuals, reflecting an excellent fit to the data and indicating that the oxidized and reduced states exhibit the same three-component fluorescence decay. The three lifetimes are completely resolved with these data as demonstrated in Figure 2. The error analysis consists of varying the parameter of interest, in this case the individual lifetime values, in an incremental manner while allowing the remaining parameters to relax to new minima while calculating the resulting χ^2. The plot of χ^2 versus the range of parameter values thus maps the error surface associated with each of the lifetimes. The intersection of the dotted lines in these plots represents the 67% (one standard deviation) and the 95% (two standard deviations) certainty level. Both the long and median lifetimes are very well resolved while the short lifetime is cleanly defined at higher lifetime values and poorly resolved on the lower edge (consistent with the distributed fitting analysis).

The results of the global analysis linking the three lifetime components across both redox state and the emission spectra are plotted in Figure 3. The fractional intensities (SAS, species-associated spectra) have been plotted for each lifetime component as a function of wavelength. The absence of pronounced wavelength dependencies indicates that each of the components displays the red-shifted, solvent-exposed, steady-state spectrum (Figure 1). The fractional intensities have been tabulated according to lifetime component and redox state to compare reduced and oxidized putidaredoxin in Table I. Rigorous error analysis was conducted on these SAS by searching their χ^2 surface, and the results indicate that the oxidized and reduced fractional intensities are not uniquely resolved (<67% confidence) with available data (data not shown). Therefore, it is impossible to state with certainty whether these differences are real or represent insignificant fitting deviations. In general, it can be noted that the oxidized and reduced proteins both contain three similar lifetime components which have been assigned to three conformational states in the next section. Small differences in the proportions of these conformations between oxidized and reduced putidaredoxin were recovered, but their physical significance is uncertain as they are not resolved in the fitting analysis.

Stern–Volmer Quenching Analysis and Assignment of Conformational Microheterogeneity. Quenching of tryptophan fluorescence in proteins can be utilized to assign particular lifetimes to physical conformations. For example, alcohol dehydrogenase exhibits a long- and a short-lifetime component and contains two tryptophans which vary greatly in their ex-

Table I: Summary of Fractional Intensities Associated with Lifetime Components as a Function of Wavelength

	long lifetime		median lifetime		short lifetime	
λ (nm)	ox	red.	ox	red.	ox	red.
330	0.713	ND[a]	0.225	ND	0.062	ND
340	0.746	0.706	0.227	0.238	0.027	0.055
350	0.754	0.738	0.221	0.219	0.025	0.044
360	0.763	0.733	0.211	0.224	0.026	0.043
370	ND	0.741	ND	0.217	ND	0.042

[a] ND, not determined at this wavelength.

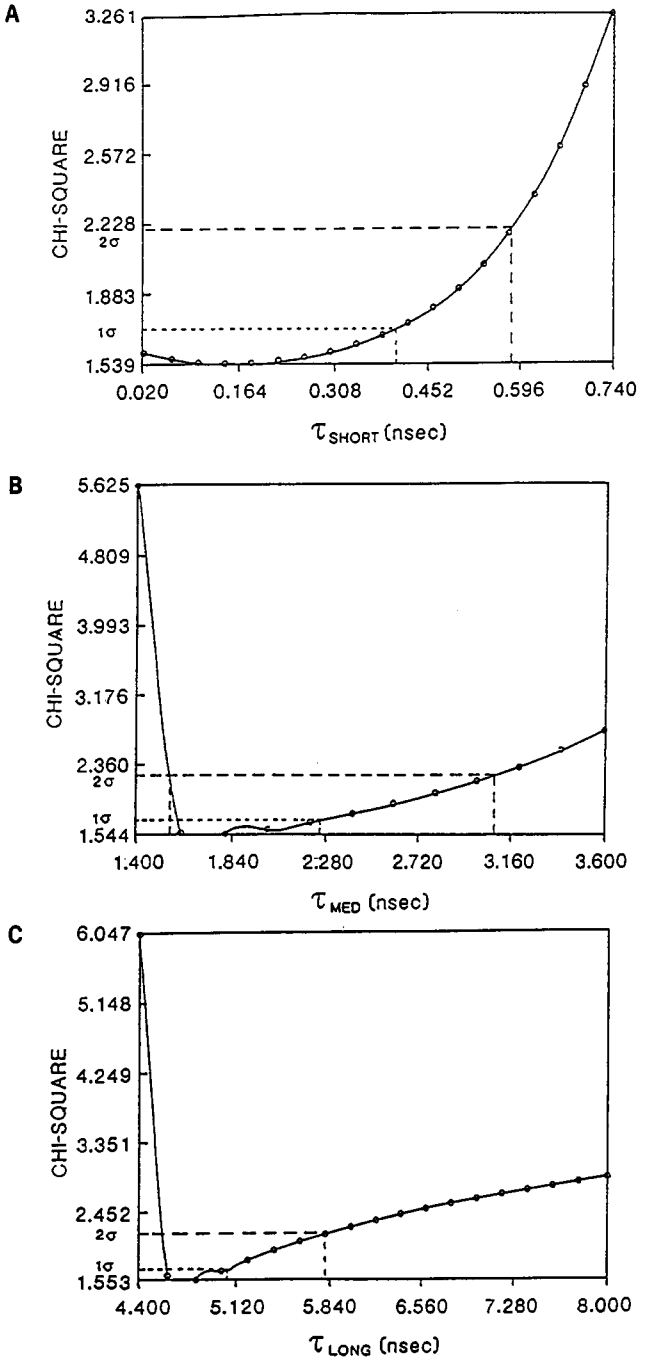

FIGURE 2: Resolution of lifetime components recovered from analysis of oxidized and reduced putidaredoxin. Confidence interval plots for (A) 0.3-ns lifetime component, (B) 1.7-ns lifetime component, and (C) 4.7-ns lifetime component. Dotted lines represent the 95% (2 σ) and 67% (1 σ) confidence limits.

posure to solvent. Quenching experiments with the external quenching agent I^- result in selective quenching of the long-lifetime component while the short-lived component remains unaltered (Ross et al., 1981). The long-lifetime component

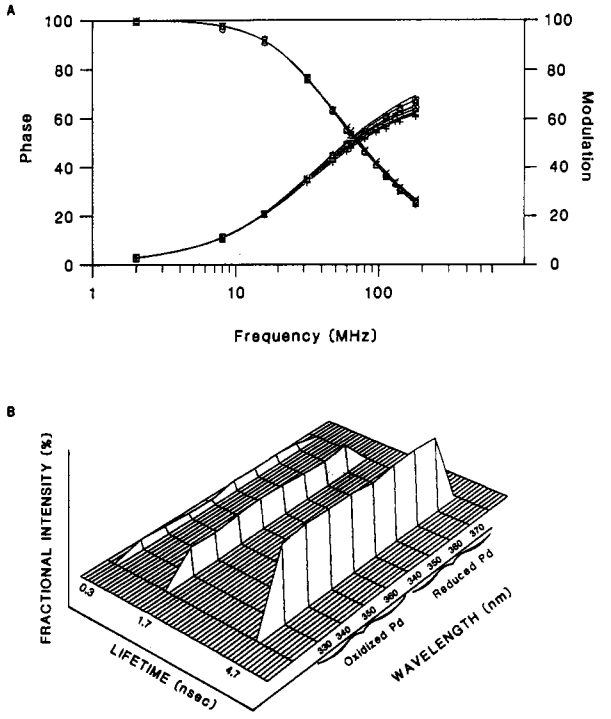

FIGURE 3: Frequency response for oxidized and reduced putidaredoxin Trp-106 fluorescence with triple-exponential global analyses across the emission spectrum. (A) Raw phase and modulation data with lines representing the best fit to a triple-exponential model with lifetimes linked across redox state and emission spectrum. The different plots, largely overlapping, represent oxidized and reduced frequency responses at the emission wavelengths shown in (B). (B) Three-dimensional graph of the lifetime and emission results from the raw data of (A), demonstrating the absence of fluorescence wavelength dependencies for oxidized and reduced putidaredoxin. The oxidized and reduced fractional intensities are plotted as a function of the three lifetime components and the emission spectrum as denoted by the wavelength numbers. The lack of meaningful fractional intensity changes across the emission spectrum demonstrates that each lifetime component displays the red-shifted steady-state spectra.

can thus be assigned to the exposed tryptophan. The large highly charged iodide ion is an excellent external quencher as its size and charge prevent its access to the hydrophobic protein interior. The putidaredoxin tryptophan fluorescence is quenched by iodide, and the effect is well described by a dynamic Stern–Volmer relationship (static quenching components did not yield acceptable fits to the data):

$$1/\tau = 1/\tau_0 + K[Q] \quad (1)$$

where τ is the lifetime, τ_0 is the lifetime in the absence of quencher, K is the Stern–Volmer quenching constant, and Q is the quencher concentration. The global analysis of quenching data at three wavelengths and five iodide concentrations, where the lifetime components are linked across the emission spectrum and the SAS of each lifetime are linked at each wavelength across the quencher range, yields a global χ^2 of 2.8. This analysis gives an easily visualized three-dimensional graph of the quenching of each of the two longer

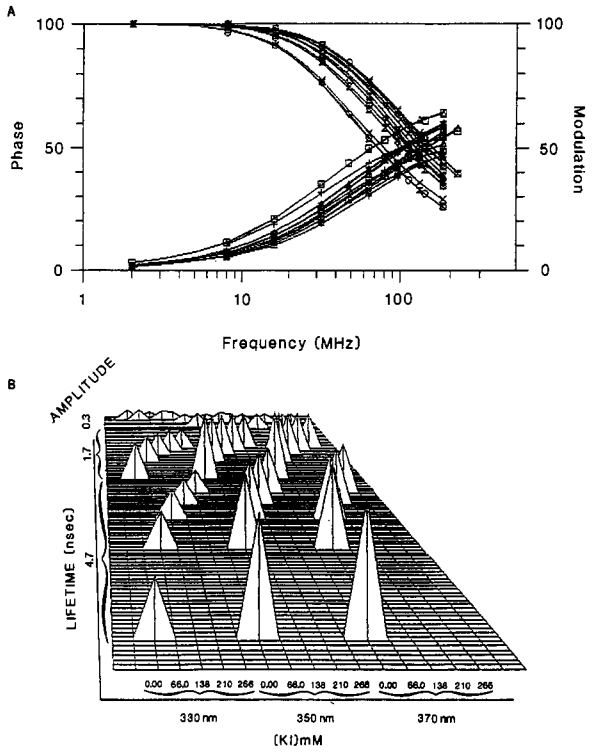

FIGURE 4: Frequency response of Trp-106 fluorescence as a function of iodide concentration. (A) Raw phase and modulation data with dynamic Stern–Volmer quenching global analysis fit for five iodide concentrations and three emission wavelengths. (B) Three-dimensional graph of global analysis results from (A), showing the Stern–Volmer dynamic quenching of the long (4.7 ns) and median (1.7 ns) lifetime components as detected at three emission wavelengths. The triangles represent the observed lifetimes at each quencher concentration, with the x-axis numbers representing iodide ion concentration. The quenching of the two longer components, at three emission wavelengths, is apparent as the shift in lifetime (triangle) position toward shorter values at increasing quencher concentration.

components by iodide ion as shown in Figure 4. The x axis is divided into three groups of five fluorescence amplitudes (triangles) representing the five iodide quencher concentrations at emission wavelengths of 330, 350, and 370 nm. The y axis represents the Trp lifetime and is divided into the three lifetime components so that the quenching effect as represented by the triangle position is proportional to iodide concentration at all three wavelengths. Both the long and median lifetimes can be seen to decrease upon iodide addition. The bimolecular quenching constants (equivalent to the Stern–Volmer bimolecular quenching constant) are 1.3×10^8 M^{-1} s^{-1} for the 4.7-ns component (k_1) and 5.9×10^8 M^{-1} s^{-1} for the 1.7-ns lifetime component (k_2). The very short lifetime is difficult to quantitate in a meaningful fashion due to its transient nature, and in these evaluations, a quenching constant was not included in the analysis. Addition of a Stern–Volmer constant to its lifetime gave a bimolecular quenching constant approximately 3 times that of the median component but did not affect the analysis to a significant extent. The quenching constants recovered in this analysis provide good evidence that the lifetime components reflect physical tryptophan conformational substates. The components are differentially quenched, and rigorous error analysis confirms that the two constants are resolved as demonstrated in Figure 5. At the 95% confidence level, k_1 limits are 7×10^7 to 1.8×10^8 M^{-1} s^{-1}, and k_2 limits are 3.6×10^8 to 1.3×10^9 M^{-1} s^{-1}.

Acrylamide, a neutral quenching agent, was utilized to test for electrostatic effects on the putidaredoxin tryptophan quenching process. A dynamic Stern–Volmer process was

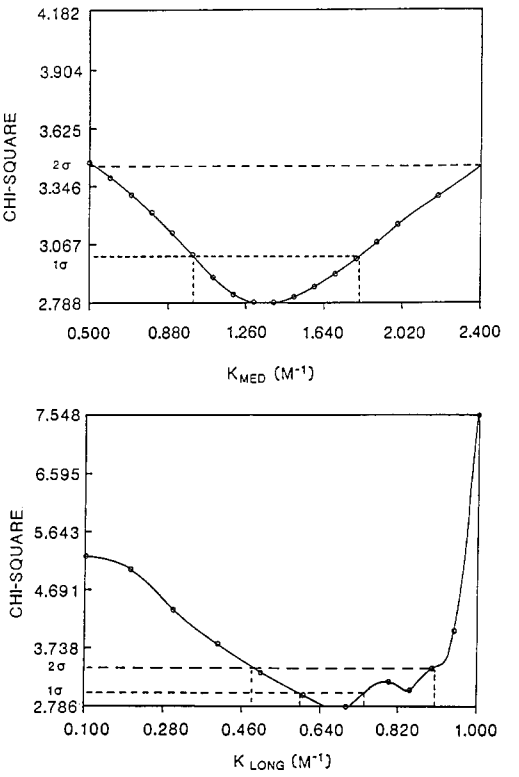

FIGURE 5: Resolution of Stern–Volmer iodide quenching constants. Confidence interval plots show the 95% and 67% confidence levels with dotted lines.

again observed, with bimolecular quenching constants of 3.3 $\times 10^8$ and 1.2×10^9 M^{-1} s^{-1} observed for the 4.7- and 1.7-ns components, respectively. The increase in absolute quenching rates with the neutral quencher suggests that electrostatic factors are influencing the quenching process. The quenching constants for these components were not uniquely resolved (<67% confidence), however, as revealed by rigorous error analysis (data not shown). This suggests that the two tryptophan conformations are not as distinguished in their accessibility to acrylamide as when compared to iodide ion, again consistent with a local electrostatic effect.

Discussion

The C-terminal tryptophan of putidaredoxin represents a specific example of a protein structural feature controlling an electron-transfer rate. Site-directed mutagenesis studies have demonstrated that an aromatic amino acid side chain is required at this position for efficient electron transfer to occur in the physiological putidaredoxin–cytochrome P-450$_{cam}$ complex (Davies et al., 1990a). A crystal structure is not available for putidaredoxin, but a high-resolution NMR solution structure is nearly complete (T. Pochapsky, personal communication), and the presence of this single tryptophan in the wild-type protein has yielded a unique opportunity for dynamic structural study of a specific residue important in an electron-transfer pathway. Steady-state fluorescence emission and polarization measurements demonstrate that this tryptophan is very solvent-exposed and rotating partially free of the bulk protein tumbling. These conclusions are further supported by the 2-D NMR data (T. Pochapsky, personal communication).

The present analysis of the tryptophan fluorescence decay strongly suggests that this tryptophan exists in three major conformational substates which are functionally characterized by differential iodide quenching accessibilities and fluorescence lifetimes. These conformational substates are present in both oxidized and reduced putidaredoxin, apparently ruling out any

gross conformational changes independent of complex formation involving the tryptophan that would be obvious candidates for structural gating of the electron-transfer process. Another possible mechanism for structural gating is a redistribution of common conformational substates, but although some fractional changes in the proportions of these conformations related to redox state were recovered from the global analysis, the statistical uncertainty of these values precludes their assignment to structural differences with present data. These studies obviously do not rule out the possibility of cytochrome P-450$_{cam}$ complex-associated conformational change that is not present in the isolated putidaredoxin redox states. Indeed, the demonstration of functionally distinguishable substates suggests possible mechanisms by which complex formation could select for an active electron-transfer geometry. For example, binding dynamics could be translated into a shift in the proportions of these substates toward the most active conformation. Redistribution of conformational substates can also lead to directional electron-transfer phenomona (Brunschwig & Sutin, 1989).

The common interpretation of differential quenching of lifetime components invokes differences in tryptophan solvent accessibility. Compilation of the correspondence between the emission λ_{max}, a general measure of solvent accessibility, and iodide quenching constants for a number of one- and two-tryptophan proteins shows a strong trend of increasing quenching activity with accessibility (Eftink, 1990). The results presented here for putidaredoxin, however, are not consistent with such a mechanism. Both the 4.7- and 1.7-ns lifetime components exhibit the red-shifted emission spectrum observed in steady-state measurements. This strongly suggests that both components are similarly solvent-exposed. Despite the apparent similarity in solvent exposure, however, the two components clearly differ in their accessibility to iodide quenching. Additionally, the absolute values of the Stern–Volmer iodide quenching constants are low given the degree of solvent exposure as estimated by the red-shifted emission spectrum (Eftink, 1990; Lakowicz & Weber, 1973). These observations are consistent with an electrostatic effect on the iodide quenching efficiency. Such effects have been observed with model indole and polypeptide compounds (Lehrer, 1971; Lakowicz & Weber, 1973) and suggested in an extrinsic protein probe system (Ando et al., 1980). In those studies, an inhibition of iodide quenching was noted for fluorophores in an anionically charged environment. Such an interpretation in the present system is supported by the studies conducted with acrylamide, where the quenching constants associated with the 4.7- and 1.7-ns conformations were greater and not uniquely resolved, suggesting both that quencher accessibility is greater with the neutral agent and that the mechanism for distinguishing iodide quenching efficiencies is not as active with the acrylamide molecule. The absolute magnitude of the quenching constants for acrylamide is also somewhat lower than would be expected for a completely solvent-exposed tryptophan residue, however (Eftink et al., 1987). Thus, there appears to be some steric constraint on quencher accessibility in addition to the electrostatic factors.

A physical model consistent with these results is shown in Figure 6. Both the 4.7- and 1.7-ns lifetime-associated conformations are solvent-exposed, as suggested by their red-shifted emission spectra. The differential iodide quenching of the two conformations can be explained by differential proximity to an anionic protein surface consisting of exposed carboxylate side chains. Such a model both provides a rationale for the differential quenching of the two lifetime components and explains the low absolute values of the Stern–Volmer quenching constants given the degree of tryptophan solvent exposure. The steady-state fluorescence polarization value is also suggestive of a tryptophan residue that is not completely constrained to global protein motion. The acrylamide quenching constants, while significantly larger than the iodide rates, are not at the diffusion-controlled limit, suggesting that some steric factors may also be present.

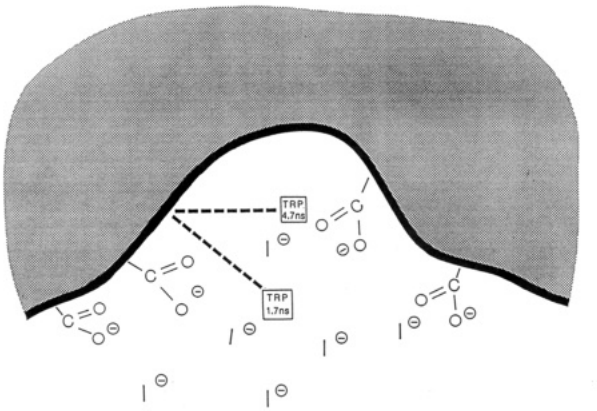

FIGURE 6: Schematic physical model proposing an electrostatically based mechanism for the differential quenching of Trp-106 conformations by iodide ion (I^-). The shaded area represents the putidaredoxin interior with the solid black line demarking the solvent-accessible surface, so that each conformation is similarly exposed to solvent. The model includes solvent-exposed Trp-106 substates (consistent with the red-shifted emission spectrum and lack of emission wavelength dependencies) that differ in their proximity to an anionic protein surface (represented by carboxylate residues) as suggested by the differential quenching rates associated with each conformation. The 4.7-ns conformation is thus pictured as lying closer to the carboxylate surface than the 1.7-ns conformation, though still exposed to solvent and the quenching agent.

In addition to satisfying the restraints imposed by the fluorescence measurements, this model is also appealing in a biological sense. Previous studies on the physiological putidaredoxin–cytochrome P-450$_{cam}$ interaction have suggested an electrostatic contribution to complex formation (Stayton & Sligar, 1990; Hintz & Peterson, 1981). A carboxylate-based putidaredoxin binding surface has been directly demonstrated with putidaredoxin reductase interactions (Geren et al., 1986) and is consistent with both the facile redox rates observed with cationic cytochrome *c* (Mock, 1977) and the observed inhibition of cytochrome b_5–cytochrome P-450$_{cam}$ binding interactions (Stayton et al., 1989). A molecular model of the cytochrome P-450$_{cam}$ binding surface responsible for putidaredoxin interactions has been suggested on the basis of this latter work, and features cationic surface charges shown to affect putidaredoxin–cytochrome P-450$_{cam}$ redox kinetics (Stayton & Sligar, 1990). The assumption that the anionic protein surface responsible for the differential iodide quenching may also be the anionic surface involved in protein–protein interactions places the essential C-terminal tryptophan directly outside of the site of cytochrome P-450$_{cam}$ interactions in position to mediate electron transfer as shown in Figure 7. This model provides a structural rationale for the requirement of an aromatic amino acid side chain at this position that may be related to potential governing roles in electron conductance, solvent exclusion, and/or selection of active complex orientation (Davies et al., 1990a; Louie et al., 1988). Future quenching studies on site-directed surface charge mutants of putidaredoxin may be used to further test this model, and also to relate the tryptophan residue to specific surface residues in three-dimensional space. In this light, preliminary determination of the solution structure of putidaredoxin by 2-D

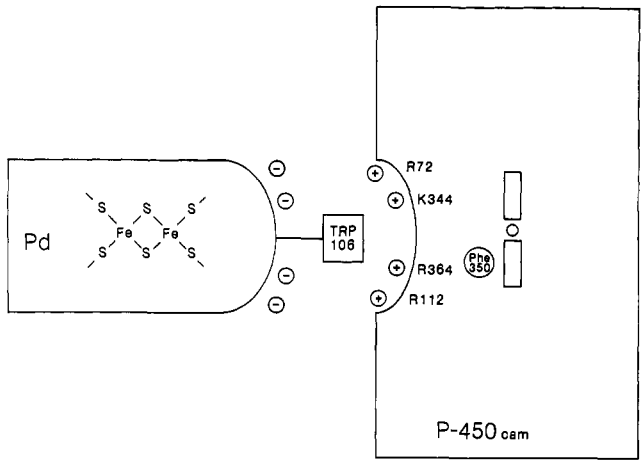

FIGURE 7: Schematic putidaredoxin–cytochrome P-450$_{cam}$ complex proposing that the anionic surface responsible for differential iodide quenching of Trp-106 is the carboxylate-based binding surface implicated in cytochrome P-450$_{cam}$ interactions. The cytochrome P-450$_{cam}$ cationic surface charges previously modeled and shown to affect putidaredoxin–cytochrome P-450$_{cam}$ electron transfer (Stayton & Sligar, 1990) are indicated along with the conserved Phe-350 residue which lies in van der Waals contact to the prosthetic heme group (also indicated). The model thus places Trp-106 at the binding interface in position to directly mediate electron transfer (Davies et al., 1990).

proton NMR techniques shows Trp-106 to be within NOE distances of portions of the carboxylate cluster (T. Pochapsky, personal communication).

ACKNOWLEDGMENTS

Most of the experiments and analyses of the fluorescence data produced were conducted at the Laboratory for Fluorescence Dynamics [LFD at the University of Illinois at Urbana–Champaign (UIUC)]. The LFD is supported jointly by the Division of Research Resources of the National Institutes of Health (RR03155-01) and the UIUC. Dr. Cathy Royer and Dr. Joseph Beechem provided invaluable assistance with equipment and analysis at the LFD. Dr. Peter Steinbach provided further assistance with data analysis, and Dr. Thomas Pochapsky kindly supplied the 2-D NMR results. We also thank Ms. Jean Lewis for expert editorial assistance.

Registry No. L-Tryptophan, 73-22-3; cytochrome P450, 9035-51-2.

REFERENCES

Ando, T., Fujisaki, H., & Asai, H. (1980) *J. Biochem. 88*, 265–276.

Bechtold, R., Kuehn, C., Lepre, C., & Isied, S. (1986) *Nature (London) 322*, 286–288.

Beechem, J. M., & Brand, L. (1985) *Annu. Rev. Biochem. 54*, 43–71.

Beechem, J. M., Gratton, E., Ameloot, M., Knutson, J. R., & Brand, L. (1990) in *Fluorescence Spectroscopy* (Lakowicz, J., Ed.) Vol. I, Plenum Publishing, New York (in press).

Brunschwig, B. S. & Sutin, N. (1989) *J. Am. Chem. Soc. 111*, 7454–7465.

Burch, A. M., Rigby, S. E., Funk, W. D., MacGillivray, R. T. A., Mauk, M., Mauk, G., & Moore, G. R. (1990) *Science 247*, 831–833.

Davies, M. D., Qin, L., Beck, J. L., Suslick, K. S., Koga, H., Horiuchi, T., & Sligar, S. G. (1990a) *J. Am. Chem. Soc. 112*, 7396–7398.

Davies, M. D., Koga, H., Horiuchi, T., & Sligar, S. G. (1990b) in *Pseudomonas: Biotransformations, Pathogenesis, and Evolving Biotechnology* (Silver, S., Ed.) pp 101–110, American Society for Microbiology, Washington, D.C.

Eftink, M. (1990) in *Fluorescence Spectroscopy* (Lakowicz, J., Ed.) Vol. I, Plenum Publishing, New York (in press).

Eftink, M., Selva, T. J., & Wasylewski, Z. (1987) *Photochem. Photobiol. 46*, 23–30.

Geren, L., Tuls, J., O'Brien, P., Millett, F., & Peterson, J. A. (1986) *J. Biol. Chem. 261*, 15491–15495.

Gratton, E., Jameson, D. M., & Hall, R. D. (1984) *Annu. Rev. Biophys. Bioeng. 13*, 105–124.

Gunsalus, I. C., & Wagner, G. C. (1978) *Methods Enzymol. 52*, 166–188.

Hazzard, J. T., McLendon, G., Cusanovich, M. A., Das, G., Sherman, F., & Tollin, G. (1988) *Biochemistry 27*, 4445–4451.

Hintz, M. J., & Peterson, J. A. (1981) *J. Biol. Chem. 256*, 6721–6728.

Hintz, M. J., Mock, D. M., Peterson, L. L., Tuttle, K., & Peterson, J. A. (1982) *J. Biol. Chem. 151*, 389–409.

Hoffman, B. M., & Ratner, M. A. (1987) *J. Am. Chem. Soc. 109*, 6237–6243.

Hopfield, J. J. (1974) *Proc. Natl. Acad. Sci. U.S.A. 71*, 3640–3644.

Jortner, J. (1976) *J. Chem. Phys. 64*, 4860–4867.

Kuki, A., & Wolynes, P. G. (1987) *Science 236*, 1647–1652.

Lakowicz, J. R., & Weber, G. (1973) *Biochemistry 12*, 4171–4179.

Lehrer, S. S. (1971) *Biochemistry 10*, 3254–3263.

Liang, N., Mauk, A. G., Pielak, G. J., Johnson, J. A., Smith, M., & Hoffman, B. M. (1988) *Science 240*, 311–313.

Louie, G. V., Pielak, G. J., Smith, M., & Brayer, G. D. (1988) *Biochemistry 27*, 7870–7876.

Marcus, R. A. (1956) *J. Chem. Phys. 24*, 966–978.

Marcus, R. A., & Sutin, N. (1985) *Biochim. Biophys. Acta 811*, 265–322.

Mclendon, G. (1988) *Acc. Chem. Res. 21*, 160–167.

McLendon, G., Pardue, K., & Bak, P. (1987) *J. Am. Chem. Soc. 109*, 7540–7541.

Miller, M. A., Hazzard, J. T., Mauro, J. M., Edwards, S. C., Simons, P. C., Tollin, G., & Kraut, J. (1988) *Biochemistry 27*, 9081–9088.

Mock, D. M. (1977) Ph.D. Dissertation, University of Texas Health Science Center at Dallas.

Nocek, J. M., Liang, N., Wallin, S. A., Mauk, A. G., & Hoffman, B. M. (1990) *J. Am. Chem. Soc. 112*, 1623–1625.

Ross, J. B., Schmidt, C. J., & Brand, L. (1981) *Biochemistry 20*, 4369–4377.

Scott, R. A., Mauk, A. G., & Gray, H. B. (1985) *J. Chem. Educ. 62*, 932–938.

Sligar, S. G., DeBrunner, P. G., Lipscomb, J. D., Namtvedt, M. J., & Gunsalus, I. C. (1974) *Proc. Natl. Acad. Sci. U.S.A. 71*, 3906–3910.

Stayton, P. S., & Sligar, S. G. (1990) *Biochemistry 29*, 7381–7386.

Stayton, P. S., Fisher, M. T., & Sligar, S. G. (1988) *J. Biol. Chem. 263*, 13544–13548.

Stayton, P. S., Poulos, T. L., & Sligar, S. G. (1989) *Biochemistry 28*, 8201–8205.

Therien, M. J., Selman, M., Gray, H. B., Chang, I.-J., & Winkler, J. R. (1990) *J. Am. Chem. Soc. 112*, 2420–2422.

van de Kamp, M., Floris, R., Hali, F. C., & Canters, G. W. (1990) *J. Am. Chem. Soc. 112*, 907–908.

Wendoloski, J. J., Matthew, J. B., & Salemme, F. R. (1987) *Science 238*, 794–797.